JOURNAL OF AIRCRAFT
Vol. 46, No. 5, September–October 2009

Numerical Simulation of Autorotation in Forward Flight

Hak Yoon Kim*
Korea Aerospace University, Goyang 412-791, Republic of Korea
Dong Jin Sheen†
Hanseo University, Seosan 360-706, Republic of Korea
and
Seung O. Park‡
Korea Advanced Institute of Science and Technology, Daejeon 305-701, Republic of Korea

DOI: 10.2514/1.42209

Autorotation in forward flight is an important subject for gyroplanes or compound helicopters. By integrating the flapping and rotational equations of motion, we investigate in this work the steady-state autorotation of a three-bladed rotor for a given set of three independent variables: forward velocity, collective pitch angle, and shaft angle. Two-dimensional aerodynamic coefficients as functions of the angle of attack and the Reynolds number from the Navier–Stokes simulation and Pitt/Peters inflow model to determine induced flowfield are adopted to implement the simulation. Transient behavior of the solution from arbitrary initial conditions to a steady-state periodic solution is described. Variations of rotor speed and flapping angle of autorotation with the shaft angle and the collective pitch angle for a given forward velocity are presented and discussed in detail. Drastic changes in the region of autorotation near a specific shaft angle is found to exist, below which the range of collective pitch angle for stable autorotation becomes very limited and the flapping angle changes abruptly with the pitch angle.

Nomenclature

B	=	tip-loss factor
b	=	number of rotor blades
$C_L(\psi)$, $C_M(\psi)$	=	rolling and pitching moment coefficients of the rotor
$C_T(\psi)$	=	thrust coefficient of the rotor
c	=	blade section chord, m
c_l, c_d	=	lift and drag coefficients of the airfoil section
d_{CM}	=	distance from the flapping hinge to the blade center of mass, m
e	=	flapping hinge offset, m
g	=	acceleration due to gravity, m/s^2
I_h	=	flapping moment of inertia of one rotor blade, kg $\cdot$ m^2
I_p	=	polar moment of inertia of complete rotor system, kg $\cdot$ m^2
n	=	index used in the summation of the number of rotor blades
R	=	rotor blade radius, m
r	=	distance measured along the blade, from the axis of rotation to the blade element, m
V	=	velocity along the flight path, m/s
$v_i(r, \psi)$	=	induced-velocity distribution; negative in the downwash sense, m/s
v_{im}	=	momentum-induced velocity at the rotor; negative in the downwash sense, m/s
v_0, v_s, v_c	=	induced-velocity harmonics, m/s
W	=	rotor blade weight, N
x	=	ratio of the blade element radius to the rotor blade radius, r/R
x_c	=	nondimensional cutout radius, r_c/R
α_s	=	rotor shaft angle (angle of attack of the disk plane), deg
β	=	rotor blade flapping angle with respect to the hub plane, rad, deg
$\beta_{\max}$, $\beta_{\min}$	=	maximum and minimum flapping angles, deg
$\dot{\beta}$, $\ddot{\beta}$	=	first and second derivatives of β with respect to time, rad/s, rad/s^2
λ_S	=	inflow ratio, $(V \sin\alpha_s - v_i)/\Omega R$
μ_S	=	advance ratio, $V \cos\alpha_s/\Omega R$
ξ	=	nondimensional hinge offset distance, e/R
ρ	=	mass density of air, kg/m^3
ψ	=	blade azimuth angle measured from a downwind position in the direction of rotation, deg
Ω, $\dot{\Omega}$	=	rotor angular velocity and acceleration, rad/s, rad/s^2

I. Introduction

AUTOROTATION in rotorcrafts is a parametrically well-defined phenomenon, as reviewed by Lugt [1]. The governing equations for the flapping and rotational motions of rotors are well established, as can be found in Johnson [2] and other references. These equations involve various dynamic properties of the rotors, complicated aerodynamics, pitch–flap coupling, hinge offset, etc. For the analysis of autorotation, these equations have often been applied so far to determine collective pitch angles iteratively under the condition that the aerodynamic torque on the rotor is zero.

Vertical autorotation is of main interest in helicopters. In a recent study [3], blade element momentum theory and a modified Froude–Finsterwalder equation for the inflow were applied for the analysis of autorotation. The flapping equation (with a flap frequency) and the inflow equation were used to design an autorotative payload delivery system in [4]. Gyroplanes and compound helicopters use autorotation during vertical and high-speed forward flights. To deal with this wide spectrum of flight conditions, cases of various advance ratios along with nonlinear and unsteady aerodynamics must be considered. McCormick [5] adopted a simplified flapping equation with a first harmonic nonuniform inflow model in his numerical study. Floros and Johnson [6] performed a numerical

Received 16 November 2008; accepted for publication 20 March 2009.

*Lecturer, Department of Aircraft Maintenance Institute, 200-1 Hwajeon-dong, Deogyang-gu; also Ph.D. Student, Korea Advanced Institute of Science and Technology, Daejeon 305-701, Republic of Korea. Member AIAA.

†Associate Professor, Department of Aeromechanical Engineering, 360 Daegok-ri, Haemi-myun.

‡Professor, Department of Aerospace Engineering, 373-1 Kusong-dong, Yuseong-gu. Senior Member AIAA.

study of a high advance ratio autorotating rotor for a compound helicopter with CAMRAD II. They adopted the homogeneous flapping equation and a slowed-rotor vehicle model. Most recently, the rotor trim problems on autorotation were studied at Georgia Institute of Technology. In their work, a Newton–Raphson iterative method to trim the rotor speed [7] and a flight dynamics model with FLIGHTLAB to trim the lightly loaded autorotating rotors [8] were used.

To deal with autorotation for advance ratios ranging from zero to beyond unity, it would be much wiser to employ a solution strategy that accounts for complex aerodynamics rather than adopting case-by-case aerodynamic models depending on the advance ratio. When the geometric configuration of a rotor with material property is given, the autorotation of the rotor is determined by aerodynamics only. For the design and operation of gyroplanes and compound helicopters, it is thus imperative to identify a steady-state autorotation for a given set of forward airspeed, collective pitch angle, and rotor shaft angle. By the steady-state autorotation, we refer to the state of autorotation in which the angular velocity Ω and the flapping angle β vary periodically with constant amplitude during the rotation, that is, $\Omega = \Omega(\psi)$ and $\beta = \beta(\psi)$. Evidently, the steady state of autorotation will depend on the combination of the three variables mentioned earlier: forward airspeed V, collective pitch angle θ_0, and rotor shaft angle α_s.

In this study, the flapping and rotational equations of motion for autorotation are integrated from an arbitrary initial state until the steady state is reached for a given set of the three variables. When the conditions for autorotation are met, the rotor speed and flapping angle variation are obtained as a periodic solution. Previously, time integration of the governing equations was introduced by Niemi [9] in his study of autorotation. However, in his study, either high-angles-of-attack cases involving reverse flow over the blade or Reynolds number effect were not dealt with. In addition, he simply employed constant induced velocity so that the variation of induced velocity with the azimuth angle and radial position were not taken into account.

To realize transient process from an arbitrary initial state to a steady-state autorotation, we use lift and drag coefficients for the entire range of angle of attack as functions of the Reynolds number. Also, we adopt a dynamic inflow model to obtain proper variations of induced velocity, so that the effective angle of attack as well as the resultant incoming velocity to the blade element can be provided. In the present study, we select a three-blade rotor model made up of NACA 0012 airfoil section for the simulation, as was done by Niemi [9]. Because one of the foci of the present work is to suggest and assess a numerical simulation method for autorotation, we select this case simply because the experimental data for comparison are available. We used two different sources of aerodynamic data for the simulation: one from the Navier–Stokes simulation and the other from available published data. It turned out that the data from the Navier–Stokes simulation performed much better. The results of the simulation are compared with the experimental data and the transient solution behavior to the steady-state rotation is described. Variations of the rotational speed and the flapping angle with the shaft and pitch angles for the steady-state autorotation at a given forward velocity are presented.

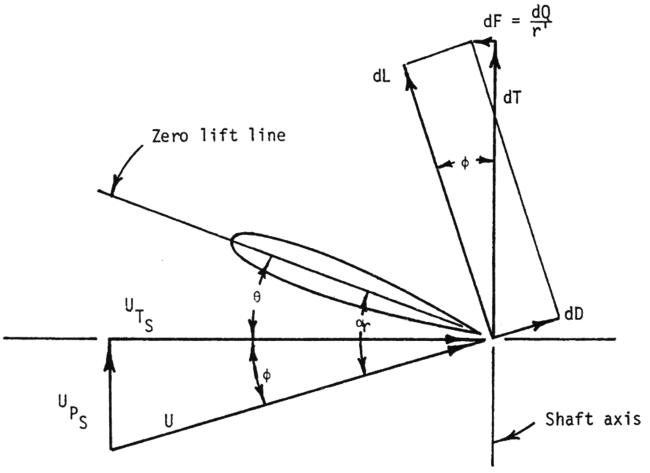

Fig. 1 Velocity and force components on a blade element.

II. Mathematical Model Description

A. Governing Equations of Autorotation

At any azimuthal position, the coupled flapping and rotational equations of motion for autorotation describe the equilibrium conditions under which the dynamic and aerodynamic moments of the rotor balance each other. The flapping equation as derived by Niemi [9] is presented here:

$$I_h[\ddot{\beta} + \sin\beta\cos\beta\Omega^2] + Wd_{\mathrm{CM}}[ge\sin\beta\Omega^2 + \sin\alpha_s\sin\beta\cos\psi + \cos\beta\cos\alpha_s] = \tfrac{1}{2}\rho c\Omega^2 R^4\left[\int_{x_c}^{B} u^2(x-\xi)c_l\cos\phi\,\mathrm{d}x + \int_{x_c}^{1.0} u^2(x-\xi)c_d\sin\phi\,\mathrm{d}x\right] \tag{1}$$

If the blade weight moment is ignored and small angle approximations ($\sin\beta \approx \beta, \cos\beta \approx 1$) are applied, the preceding equation can be simplified significantly [10]. However, we use Eq. (1), because the simplifying assumptions are not well justified for the present problem. In the derivation of the preceding form, in-plane motion and pitch–flap coupling were ignored.

The rotational equation of motion, with the assumption that the polar moment of inertia of the rotor system is constant, is given as

$$I_P\dot{\Omega} = \tfrac{1}{2}\rho c\Omega^2 R^4\sum_{n=1}^{b}\left[\int_{x_c}^{B} u^2 c_l\sin\phi[\xi + (x-\xi)\cos\beta]\,\mathrm{d}x - \int_{x_c}^{1.0} u^2 c_d\cos\phi[\xi + (x-\xi)\cos\beta]\,\mathrm{d}x\right]_{\psi+\frac{2\pi(n-1)}{b}} \tag{2}$$

The rotor angular velocity Ω and the flapping angle β can be determined by integrating Eqs. (1) and (2) simultaneously. For the integration, aerodynamic terms have to be calculated first. Each blade element encounters a nondimensional velocity $u = (u_{P_S}^2 + u_{T_S}^2)^{1/2}$, where u_{P_S} and u_{T_S} are, respectively, the perpendicular and tangential velocity components to the plane of rotation, as shown in Fig. 1. The two velocity components can be expressed in terms of the inflow ratio and the advance ratio as follows:

$$u_{P_S} = \lambda_S\cos\beta - \mu_S\cos\psi\sin\beta - (x-\xi)\dot{\beta}/\Omega \tag{3}$$

$$u_{T_S} = [\xi + (x-\xi)\cos\beta] + \mu_S\sin\psi \tag{4}$$

The inflow angle is simply given by $\phi = \tan^{-1}(u_{P_S}/u_{T_S})$. When no blade twist is present, the effective angle of attack of a blade element is given by $\alpha_r = \theta_0 + \phi$, where θ_0 is the collective pitch angle. The lift and drag coefficients of the blade element are obtained from the solution of the two-dimensional Navier–Stokes equation, a brief outline of which is described later. As implied in Eq. (3), calculation of induced velocity v_i is essential to determine u_{P_S}. The induced velocity for a given blade element location and azimuth angle is computed in this work as described next.

B. Induced-Velocity Field

Various models and methodologies, including the old Glauert model [11] and the recent model by Morillo and Peters [12], have been developed to estimate induced velocities. Summaries on various induced-velocity models are given in [13,14]. The Pitt/Peters inflow model [15] was used by Houston in his study of the autogyro stability problem [16], and we adopt a static form of this model in the present work. At any radial and azimuth station, the induced velocity is decomposed into the following three components:

$$v_i(r,\psi) = v_0 + v_s(r/R)\sin\psi + v_c(r/R)\cos\psi \tag{5}$$

The three components of harmonics v_0, v_s, and v_c are calculated from the following equation:

$$\begin{Bmatrix} v_0 \\ v_s \\ v_c \end{Bmatrix} = [L] \begin{Bmatrix} C_T \\ C_L \\ C_M \end{Bmatrix} \tag{6}$$

The static gain matrix $[L]$ is given as

$$[L] = \frac{1}{v_m} \begin{bmatrix} \frac{1}{2} & 0 & \frac{15\pi}{64}\sqrt{\frac{1-\sin\chi}{1+\sin\chi}} \\ 0 & \frac{-4}{1+\sin\chi} & 0 \\ \frac{15\pi}{64}\sqrt{\frac{1-\sin\chi}{1+\sin\chi}} & 0 & \frac{-4\sin\chi}{1+\sin\chi} \end{bmatrix} \tag{7}$$

In the preceding matrix, the wake mass velocity v_m is given by $v_m = [\mu_s^2 + \lambda_s(\lambda_s + v_{im})]/v_T$, where $v_T = (\mu_s^2 + \lambda_s^2)^{1/2}$ is referred to as wake velocity. The skew angle χ is determined from the relation $\chi = \tan^{-1}(|\lambda_s|/\mu_s)$. As Houston [16] pointed out, v_m and v_T are always positive for the case of autorotation, signifying that the wind flows toward the rotor disk plane forming a wake above the disk plane. The original Pitt/Peters inflow model [15] is a dynamic model which contains first-order derivatives of induced-velocity components with respect to ψ. As mentioned already, we neglect these derivative terms, as in Eq. (6), by assuming that the induced velocity changes slowly with ψ.

C. Two-Dimensional Navier–Stokes Analysis of Airfoil Aerodynamics

To integrate Eqs. (1) and (2), the aerodynamic coefficients of the blade element must be supplied. The inflow model described earlier provides the effective angle of attack and the resultant velocity for each blade element. Lift and drag coefficients also need to be provided to evaluate the aerodynamic terms of Eqs. (1) and (2). Niemi [9] used aerodynamic coefficients from the experimental data that was then available. However, the angle-of-attack range of the data was rather limited. Sheldahl and Klimas [17] compiled a huge amount of aerodynamic data of the NACA 0012 airfoil over a very wide range of angle of attack and the Reynolds number. We first adopted these data for the simulation. However, we found that the discrepancy was rather large between the angular velocity or rpm from the simulation results and that of the experimental data of Niemi [9]. We thus came to an idea that the aerodynamic data may better be supplied from the Navier–Stokes simulation for better accuracy. It will be shown later that the aerodynamic data from the Navier–Stokes simulation indeed produce better results.

To obtain aerodynamic data in the form $c_l = c_l(\alpha_r, Re)$ and $c_d = c_d(\alpha_r, Re)$ for the NACA 0012 airfoil from the Navier–Stokes simulation, FLUENT 6.2 was used. Because the NACA 0012 airfoil is symmetric, computations were carried out in every 2-deg interval from 0 to 180 deg over the Reynolds number range of $10^4 \le Re \le 10^7$. The flow was assumed to be laminar when $Re < 2\times10^5$ and turbulent when $Re > 2\times10^6$. For turbulent flow simulation, we adopted the κ-ε model, and used a simple linear interpolation to obtain c_l and c_d when $2\times10^5 < Re < 2\times10^6$.

D. Simulation Procedure

To identify a steady-state autorotation for a given set of three variables (α_s, θ_0, V), Eqs. (1) and (2) are integrated in time with arbitrary initial values of Ω, β, and $\dot\beta$; the variations of Ω and β with time (or equivalently azimuth angle) are monitored. To update the induced-velocity field, C_T, C_L, and C_M as functions of ψ are evaluated from the aerodynamic data. At the first step of the integration, these data are not available, therefore we set $C_L = C_M = 0$, and estimate C_T by using

$$C_T = \frac{\sigma a}{2}\left[\frac{\theta_0}{3} + \frac{\mu_s^2\theta_0}{2} + \frac{\lambda_s}{2}\right] \tag{8}$$

where σ is the rotor solidity and a is the lift curve slope. The steady-state autorotation is judged by a continuous monitoring of $\Omega(\psi)$ and $\beta(\psi)$ to examine whether they behave periodically with constant amplitude or not.

III. Results

The present simulation is performed, as mentioned already, for the case of a three-blade rotor model that was studied both experimentally and numerically by Niemi [9]. Details of the rotor are given in Table 1. For the simulation, the rotor blade was divided into 50 elements. For the time integration of equations of motion, Δt was set to 10^{-4} s.

A. Importance of Initial Conditions

To examine the dependence of the solution on initial conditions, we selected two cases of flow conditions as test cases: ($\alpha_s = 21$ deg, $\theta_0 = 2$ deg, $V = 17.7$ m/s) and ($\alpha_s = 13$ deg, $\theta_0 = 0$ deg, $V = 17.7$ m/s). These cases were found to sustain steady-state autorotation in Niemi's experiment [9]. Figure 2 illustrates typical solution curves that converge to steady-state values after a transitional period. The initial rpm was set at 2270, which was the angular velocity of the autorotation for the case of $\alpha_s = 21$ deg in Niemi's experiment. C_T values at $t = 0$ of Fig. 2 were computed from Eq. (8). Whereas Fig. 2 demonstrates a converging case of simulation, Fig. 3 shows two different cases: one that converges to steady state and the other that diverges. In Fig. 3, we present time evolution of the maximum and minimum flapping angle ($\beta_{\max}$ and $\beta_{\min}$) for the two cases. From $\beta_{\max}$ and $\beta_{\min}$, which are referenced to the hub plane, the rotor disk tilt or the coning angle can be easily estimated. When the initial rpm was set at 2270 or 2000, we see that the solution proceeds to the steady-state autorotation. On the contrary, when the initial rpm was set at 1500, the solution diverges: the flapping angle increases continuously and the angular velocity decreases. We conjecture that the centrifugal force term at 1500 rpm is not large enough to return the blade to the plane of rotation against the aerodynamic force term. Hence, the amplitude of the flapping angle ($\beta_{\max}$ and $\beta_{\min}$ in Fig. 3) increases rapidly. Increase of the flapping angle results in a decrease of the angular velocity, which in turn causes further increase of the flapping angle, as evidenced by line b in Fig. 3. It is thus recommended that we select the initial rpm to be greater than the expected rpm of autorotation for successful simulation.

Transient behavior of β from different initial flapping angles is shown in Fig. 4 for the case of ($\alpha_s = 13$ deg, $\theta_0 = 0$ deg, $V = 17.7$ m/s). The initial rpm and $\dot\beta$ were 2270 and 0, respectively. The flapping angle variations of a specific blade are shown in the figure. We see that the periodic solution has been reached in about 0.15 s regardless of initial values of β. The initial flapping angle of 3 deg seemed too large when compared with the steady-state solution. However, a high value of initial rpm was good enough to reduce β sufficiently, so that a converged solution was reached in this

Table 1 Geometric and inertia characteristics of rotor model

Parameter	Value
Diameter	0.92 m
Number of blades	3
Chord	0.05 m
Solidity, σ	0.104
Airfoil section	NACA 0012
Blade pitch angle (collective pitch)	Variable
Blade twist	None
Cutout radius	0.08 m
Flapping hinge offset	0.025 m (5.5% radius)
Blade weight moment	0.3 N · m
Blade flapping inertia	0.008 kg · m^2
Polar moment of inertia (blades and hub)	0.029 kg · m^2
Lock number, γ	2.1
Tip-loss factor, B	0.99

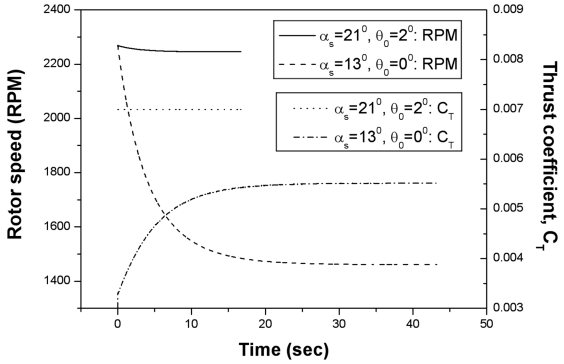

Fig. 2 Variation of rotor speed and thrust coefficient.

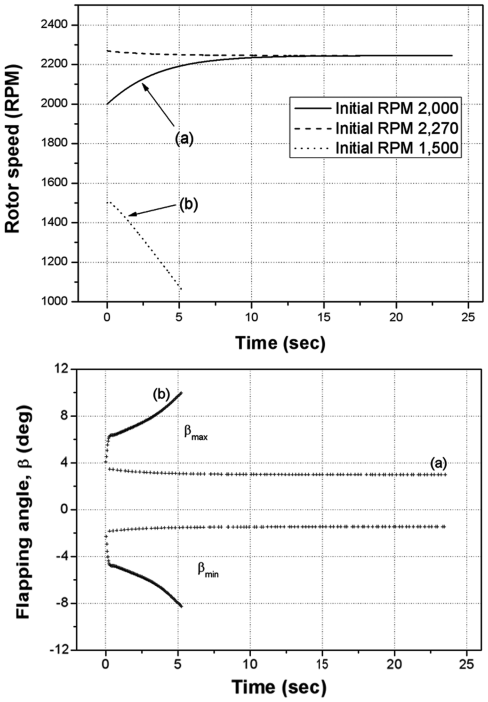

Fig. 3 Effect of different initial revolutions per minute: line a shows flapping convergence, line b shows flapping divergence; $\alpha_s = 21$ deg, $\theta_0 = 2$ deg, and $V = 17.7$ m/s.

case. In contrast to Fig. 4, we present a case of flapping divergence in Fig. 5 where variations of $\beta_{\max}$ and $\beta_{\min}$ with time are plotted. The aerodynamic condition of Fig. 5 is ($\alpha_s = 6$ deg, $\theta_0 = 0$ deg, $V = 17.7$ m/s). It was found in Niemi's experiment [9] that $\alpha_s = 6$ deg and $\theta_0 = 0$ deg were too small to sustain autorotation. Even if

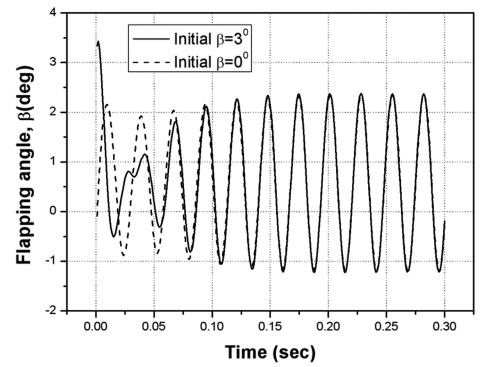

Fig. 4 Transient behavior of flapping angle; $\alpha_s = 13$ deg, $\theta_0 = 0$ deg, and $V = 17.7$ m/s.

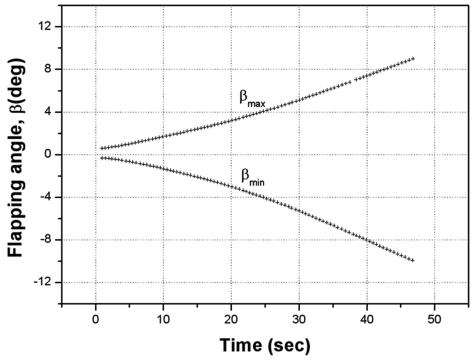

Fig. 5 Flapping divergence; $\alpha_s = 6$ deg, $\theta_0 = 0$ deg, and $V = 17.7$ m/s.

we started the simulation with an initial rpm of 2270, the solution proceeded to flapping divergence as it should.

Figures 3–5 suggest that the flapping angle β is a good indicator to judge whether the simulation will converge to a steady-state autorotation or not. In all of the simulation cases presented in this work, we use the condition of $|\beta| < 5$ deg as a judging criterion to identify a stable autorotation.

B. Typical Blade Motion During Autorotation

Figure 6 shows typical flapping angle variations of autorotation of the three-blade rotor of the present simulation. The initial conditions were rpm $= 2270$, $\beta = \dot{\beta} = 0$. We see that all three blades went into stable periodic motion (Fig. 6b) in about 0.15 s (Fig. 6a). At time $t = 0$, the azimuth angle of the number one blade is zero (this is how the no. 1 blade is defined). From Figs. 6b and 7, we find that the flapping motions of the three blades are essentially the same except for the presence of phase lag, as expected. As the rotor rotates counterclockwise (viewed from above), the no. 3 blade follows the no. 1 blade with a phase-angle difference of 120 deg, and the no. 2 blade follows the no. 3 blade in exactly the same manner. The maximum flapping angle of the no. 1 blade occurs at around $\psi = 180$ deg when the blade tip faces the forward velocity, as expected (Fig. 7). Figure 8 presents the angular velocity of the rotor together with the flapping angle variation. We clearly see that the angular velocity varies periodically even though the amplitude is small. Obviously, the period of the rotor speed variation is only one-third of the period of the flapping angle variation of one blade because we have three blades in this rotor.

C. Comparison with Experimental Data

The present simulation method employs a dynamic induced-velocity model and two-dimensional airfoil data. It is therefore necessary to investigate the accuracy and adequacy of the present method against the experimental data. Figure 9 shows two groups of rotor speed curves obtained in the present simulation, together with the experimental data of Niemi [9]. One group of curves represents the results obtained by using the airfoil data from [17] and the other group by using data from the Navier–Stokes solution of the present work. The initial conditions for all of the simulation cases were the same: rpm $= 2270$, $\beta = \dot{\beta} = 0$. Figure 9 indicates that the airfoil data from the present Navier–Stokes solution perform better, yielding much closer steady-state rotational speeds to the experimental values. We also see that the rotational speed is almost linearly proportional to the rotor shaft angle. Increase of pitch angle at a given shaft angle is seen to increase the rotational speed. However, the relation seen in this figure is far from being linear. To generate the data of Fig. 9, it was necessary to establish judgment criteria to identify steady-state autorotation. For the present rotor, it was found suitable to terminate the computation when the flapping angle exceeded ± 5 deg as it marked the starting of flapping divergence (see Fig. 3). We judged that the steady-state autorotation was achieved when the change of average rotor speed over one revolution was less than 0.1 rpm during 3 s, that is, $\Delta\text{rpm}_{3s} < 0.1$. Figure 10 compares

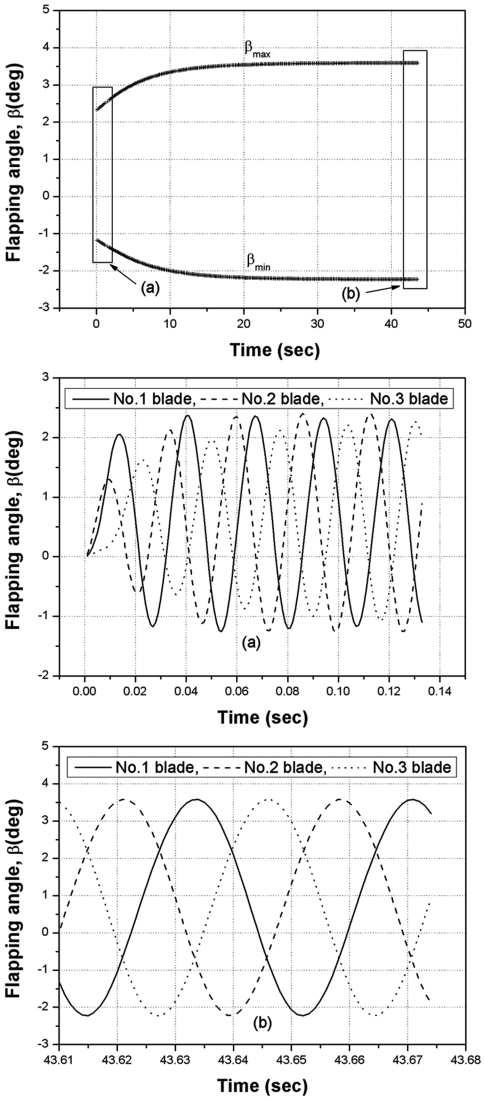

Fig. 6 Flapping angle variations: line a shows transient state, line b shows periodic steady state; $\alpha_s = 13\,\text{deg}$, $\theta_0 = 0\,\text{deg}$, and $V = 17.7\,\text{m/s}$.

the flapping angles of the present simulation with the experimental data at $\psi = 0$ and $\psi = 180\,\text{deg}$. Our computational results show that the flapping amplitude increases with the collective pitch angle. However, the experimental data shown does not show this tendency. The flapping angle was smallest when $\theta_0 = 0\,\text{deg}$, but largest when $\theta_0 = 1\,\text{deg}$ not when $\theta_0 = 2\,\text{deg}$. Considering the difficulties in measuring the flapping angle [9], we conjecture that the experimental data might not have been accurate enough. It is rather straightforward

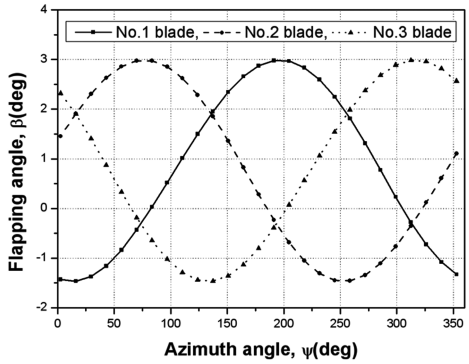

Fig. 7 Flapping angle distribution over azimuth angle; $\alpha_s = 21\,\text{deg}$, $\theta_0 = 2\,\text{deg}$, and $V = 17.7\,\text{m/s}$.

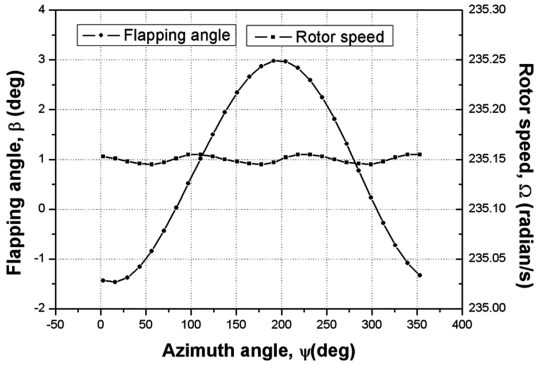

Fig. 8 Rotor speed (angular velocity) and flapping angle of no. 1 blade; $\alpha_s = 21\,\text{deg}$, $\theta_0 = 2\,\text{deg}$, and $V = 17.7\,\text{m/s}$.

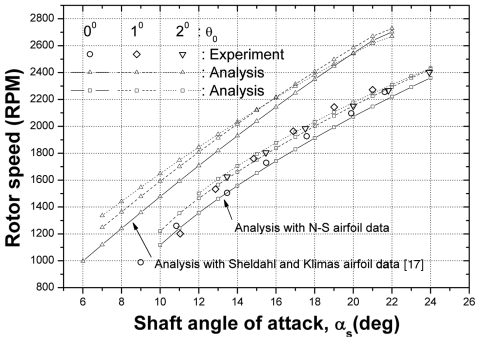

Fig. 9 Comparison of rotor speed with experimental data.

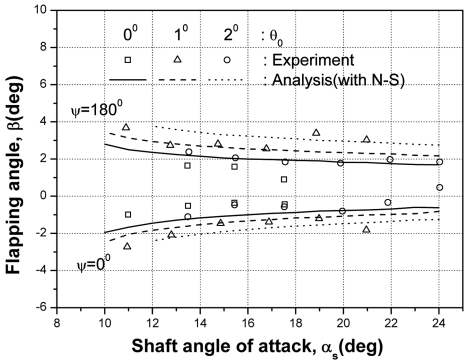

Fig. 10 Comparison of flapping angle at $\psi = 180\,\text{deg}$ and $\psi = 0\,\text{deg}$.

to anticipate that the aerodynamic force that causes an increase of the flapping angle becomes greater as the collective pitch angle increases.

D. Steady Autorotation Range

A natural question in the study of autorotation is to identify a region where autorotation is sustained. In this section, we pursue this question at the forward velocity of 17.7 m/s. The rotor shaft angle and the collective pitch angle were input in the range $0 \le \alpha_s \le 15\,\text{deg}$ and $-10 \le \theta_0 \le 4\,\text{deg}$, respectively. Initial rotor rpm was set at 2270 for all the cases with $\beta = \dot{\beta} = 0$. For the calculation, we used $\Delta t = 10^{-4}$ s, $\Delta\alpha_s = 1\,\text{deg}$, and $\Delta\theta_0 = 0.2\,\text{deg}$. For a given value of α_s, the collective pitch angle was decreased to determine the range of pitch angle in which steady autorotation is maintained. As has been stated earlier, the criterion of the steady-state autorotation in the simulation was that the magnitude of flapping angle was less than 5 deg. Figure 11 summarizes the results of the present computation. From Fig. 11, we notice two major trends: the range of pitch angle for autorotation gets narrower as the shaft angle decreases, and the angular velocity of autorotation increases almost linearly with the

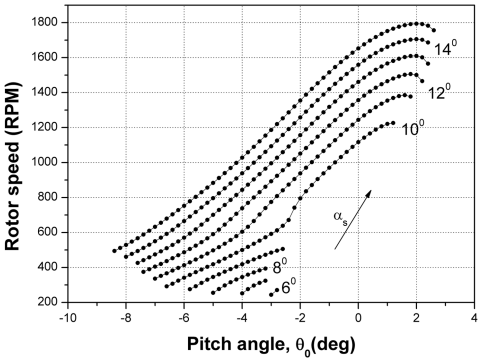

Fig. 11 Rotor speed variation at $-5 < \beta < 5$ deg for three variables: $0 \le \alpha_s \le 15$ deg, $-10 \le \theta_0 \le 4$ deg, and $V = 17.7$ m/s.

pitch angle for a given shaft angle. The latter tendency, however, no longer holds near the maximum pitch angle (See the curves near the $\theta_0 = 2$ deg line. See also Fig. 9). It is worthwhile to note that the range shrinks drastically when the shaft angle changes from 10 to 9 deg. The reason for this is not yet clear at present. We only infer vaguely that there must be a critical aerodynamic parameter, such as lift-to-drag ratio, that distinguishes these two groups of curves because the shaft angle and the pitch angle are major variables to determine local angle of attack [Eqs. (3) and (4)]. Investigation on this is left for further study. Advance ratios corresponding to Fig. 11 are shown in Fig. 12. As the forward velocity is fixed, the advance ratio is determined by the rotational speed and the shaft angle in this case. Thus, Fig. 12 is more or less an inversed version of Fig. 11. At around the point of $\theta_0 = -2$ deg and $\alpha_s = 10$ deg, which is a region where the curve behaves in a peculiar manner, the advance ratio is approximately 0.5. When $\alpha_s = 9$ deg, no autorotation is seen to be sustained at $\theta_0 = -2$ deg. For advance ratios above 0.5, the reverse flow area of the retreating blade becomes significant, as is well known in rotor aerodynamics. Again, this sudden change in tendency is left out for further study.

Variations of the maximum flapping angle $\beta_{\max}$ for various combinations of shaft and pitch angles are shown in Fig. 13. When the $\beta_{\max}$ value increases, the rotor disk plane (i.e., tip path plane) inclines backward even more, causing lift-drag ratio of the rotor to deteriorate. However, we find from Fig. 11 that the rotational speed corresponding to the pitch angle at which $\beta_{\max}$ is minimal is rather small. This signifies that a compromise needs be made between the rotational speed and $\beta_{\max}$ to choose a pitch angle for best performance. We also note from Fig. 13 that drastic change in $\beta_{\max}$ distribution also occurs when the shaft angle changes from 10 to 9 deg, as is the case in Fig. 11. This suggests that the choice of pitch angle for a given shaft angle or vice versa for practical cases should be carefully made, for which numerical simulation in advance may be of great help.

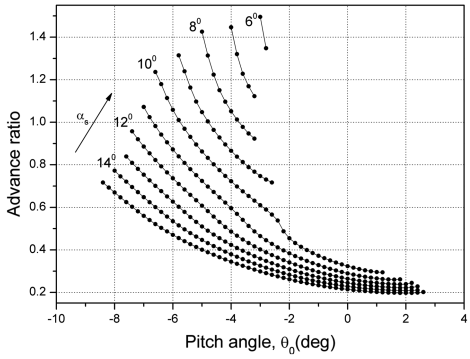

Fig. 12 Advance ratio variation at $-5 < \beta < 5$ deg for three variables: $0 \le \alpha_s \le 15$ deg, $-10 \le \theta_0 \le 4$ deg, and $V = 17.7$ m/s.

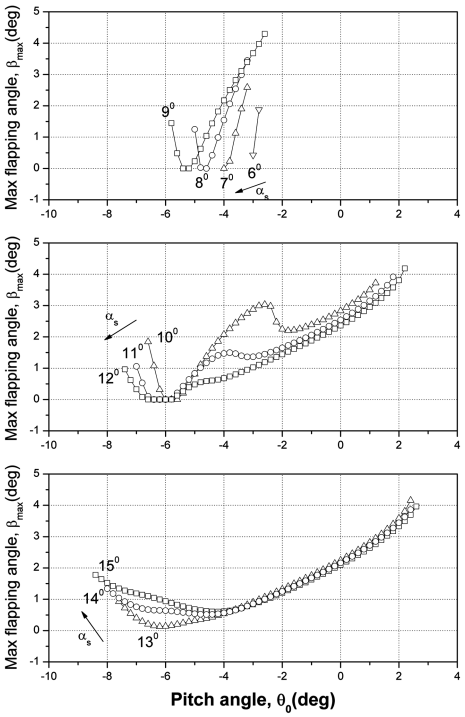

Fig. 13 Variation of maximum flapping angle: $0 \le \alpha_s \le 15$ deg, $-10 \le \theta_0 \le 4$ deg, and $V = 17.7$ m/s.

IV. Discussion

To the authors' knowledge, it was Niemi [9] who first numerically solved the coupled equations, the rotational and flapping equations of rotor to study autorotation. The present work is an extension of Niemi's work in the sense that we integrate the coupled governing equations of motion. We use aerodynamic coefficients for the blade airfoil from the Navier–Stokes simulation over the entire range of angle of attack and over a broad range of Reynolds number covering both the laminar and turbulent flows. We also adopt the Pitt/Peters inflow model [15] to determine the induced-velocity field as the computation proceeds. These two features distinguish the present work from that of Niemi [9]. We have seen in Fig. 9 that the present method generates better data than the other case when compared with the experimental data of Niemi. We conjecture that this close agreement could have been caused by the aerodynamic data at low Reynolds numbers. In most cases of the present simulation, the Reynolds number was less than 10^6. We recall here that the chord length of the rotor model in the present simulation is only 5 cm (Table 1). In this sense, a rotor of larger scale may offer a different viewpoint than this work. For a higher airspeed, we may encounter situations where the aerodynamic data with compressible correction need to be provided.

Even though the present simulation is for a model rotor of rather small size, the results obtained bear some practical significance. Collective pitch angle and shaft angle are the two major control variables for autorotation. The data contained in Figs. 11 and 13 signify that the trimming points of autorotation toward a desired rpm with moderate flapping angle can be efficiently found with the aid of numerical simulation.

V. Conclusions

A systematic numerical method to identify steady-state autorotation in forward flight for a given set of forward velocity, collective pitch, and shaft angle was presented, and the results of simulation for a three-bladed rotor with a NACA 0012 airfoil were given. The proposed scheme employed two-dimensional aerodynamic data from the Navier–Stokes simulation and a dynamic inflow model. For the present example case, the use of Navier–Stokes data yielded better results than the experimental data available. It was found that

the initial rotor speed higher than the expected rotor speed of a steady-state autorotation should be specified at the start of calculation for successful computation. Variations of rotor speed of autorotation with the collective pitch angle and shaft angle were presented for the present rotor model. The results indicated that the rotor speed increased with the collective pitch angle for a given shaft angle, and the range of collective pitch angle over which autorotation was possible became wider as the shaft angle was increased. It was also found that there was a critical shaft angle: the range of pitch angle for stable autorotation shrank drastically when the shaft angle was smaller than this critical angle.

References

[1] Lugt, H. J., "Autorotation," *Annual Review of Fluid Mechanics*, Vol. 15, Jan. 1983, pp. 123–147. doi:10.1146/annurev.fl.15.010183.001011

[2] Johnson, W., *Helicopter Theory*, Dover, New York, 1980, pp. 184–262.

[3] Cuerva, A., Sanz-Andres, A., Meseguer, J., and Espino, J. L., "An Engineering Modification of the Blade Element Momentum Equation for Vertical Descent: An Autorotation Case Study," *Journal of the American Helicopter Society*, Vol. 51, No. 4, 2006, pp. 349–354. doi:10.4050/JAHS.51.349

[4] Brindejonc, A., Sirohi, J., and Chopra, I., "Design and Testing of an Autorotative Payload Delivery System," *Journal of the American Helicopter Society*, Vol. 52, No. 4, 2007, pp. 360–370. doi:10.4050/JAHS.52.360

[5] McCormick, A. W., "A Numerical Analysis of Autogyro Performance," AIAA Paper 2002-5950, Nov. 2002.

[6] Floros, M. W., and Johnson, W., "Stability and Control Analysis of the Slowed-Rotor Compound Helicopter Configuration," *Journal of the American Helicopter Society*, Vol. 52, No. 3, 2007, pp. 239–253. doi:10.4050/JAHS.52.239

[7] Schank, T., "Optimal/Weroelastic Trim for Rotorcraft with Constrained, Non-Unique Trim Solutions," Ph.D. Thesis, School of Aerospace Engineering, Georgia Inst. of Technology, Atlanta, GA, April 2008.

[8] Rigsby, J. M., "Stability and Control Issues Associated with Lightly Loaded Rotors Autorotating at High Advance Ratios," Ph.D. Thesis, School of Aerospace Engineering, Georgia Inst. of Technology, Atlanta, GA, Oct. 2008.

[9] Niemi, E. E., Jr., "A Method for Determining the Effects of Rapid Inflow Changes on the Dynamics of an Autorotating Rotor," Ph.D. Dissertation, Dept. of Mechanical and Aerospace Engineering, Univ. of Massachusetts Amherst, MA, April 1974.

[10] Leishman, J. G., *Principles of Helicopter Aerodynamics*, Cambridge Univ. Press, New York, 2000, p. 135.

[11] Glauert, H. A, "General Theory of the Autogyro," British Aeronautical Research Council Rept. and Memo. No. 1111, 1926.

[12] Morillo, J. A., and Peters, D. A., "Velocity Field Above a Rotor Disk by a New Dynamic Inflow Model," *Journal of Aircraft*, Vol. 39, No. 5, 2002, pp. 731–738. doi:10.2514/2.3019

[13] Chen, R. T. N., "A Survey of Non-Uniform Inflow Models for Rotorcraft Flight Dynamics and Control Applications," *Vertica*, Vol. 14, No. 2, 1990, pp. 147–184.

[14] Gaonkar, G. H., and Peters, D. A., "A Review of Dynamic Inflow Modeling for Rotorcraft Flight Dynamics," *Vertica*, Vol. 12, No. 3, 1988, pp. 213–242.

[15] Peters, D. A., and HaQuang, N., "Dynamic Inflow for Practical Applications," *Journal of the American Helicopter Society*, Vol. 33, No. 4, 1988, pp. 64–68. doi:10.4050/JAHS.33.64

[16] Houston, S. S., "Validation of a Rotorcraft Mathematical Model for Autogyro Simulation," *Journal of Aircraft*, Vol. 37, No. 3, 2000, pp. 403–409. doi:10.2514/2.2640

[17] Sheldahl, R. E., and Klimas, P. C., "Aerodynamic Characteristics of Seven Airfoil Sections Through 180 Degrees Angle of Attack for Use in Aerodynamic Analysis of Vertical Axis Wind Turbines," Sandia National Lab., Rept. SAND80-2114, March 1981.